Fast Solutions of the 2D Inverse Scattering Problem Based on a TSVD Approximation of the Internal Field for the Forward Model

Paul-André Barrière, Jérôme Idier, *Member, IEEE*, Yves Goussard, *Member, IEEE*, and Jean-Jacques Laurin, *Senior Member, IEEE*

***Abstract*—An alternative formulation of the microwave tomography problem is proposed, in order to reduce the computation time of the inversion procedure. The well-known multiplicative regularized contrast source inversion method is used as reference algorithm. Our formulation is based on a truncated singular value decomposition of the matrix involved in the most computationally intensive operations of the inversion algorithm. After theoretical and practical investigation of the behavior of the singular values, it is shown that the corresponding approximation does not yield any significant degradation of the quality of the solutions even for large complex permittivity contrasts, while the computation times are reduced by a factor ranging between 1.1 and 6 with respect to the original method.**

***Index Terms*—Contrast source inversion, microwave tomography, nonlinear inversion, singular value decomposition.**

I. Introduction

THE goal of microwave tomography is to provide a quantitative estimate of the permittivity and conductivity distribution of an unknown object under test. Biomedical imaging and more precisely breast cancer detection [1]–[3] are quite promising fields of application. However, if clinical applications are considered, the computation time becomes a critical issue.

Due to the nonlinearity and ill-posed nature of the problem [4], existing algorithms offer a range of trade-offs between the computation cost and the ability to deal with problems involving large scatterers. A good compromise between computation time and robustness can be obtained by methods that account for the nonlinearity of the problem but are based on local optimization schemes. It is the case for the distorted Born iterative method (DBIM) [5] (which is equivalent to the Newton-Kantorovich [6] and Levenberg-Marquardt [7] methods), the contrast source-extended Born (CS-EB) inversion method [8], [9] and the multiplicative regularized contrast source inversion (MR-CSI) method [10]–[15] (which is an extension to the original CSI method [16]).

A drawback of DBIM is that solving of the forward problem is required at each iteration, which is computationally burdensome. An attempt to overcome this problem is proposed in [17], [18] where a DBIM is used with a fast forward solver.

The objective of the CS-EB formulation is to reduce the *degree of nonlinearity* of the problem. In [9], it is coupled with a linear sampling method [19] and the resulting algorithm presents improved performance, notably from the computation time point of view. However, the conclusion of the authors is that further works on the computational efficiency of the method are still desirable. Note that CS-EB can also be used for efficient computation of the forward problem [20].

This paper deals with the MR-CSI approach which presents a relatively low computational cost per iteration and, contrarily to DBIM, does not require solving the forward problem. However, it may require a significantly larger number of iterations; therefore, strategies to reduce the computation time remain highly desirable.

Here, we propose to reduce the volume of computation of the MR-CSI method by using an approximate and parsimonious representation of the microwave tomography problem. More precisely, the reduction is achieved by using a truncated singular value decomposition (SVD) of the largest matrix involved in the problem formulation. First, the relevance and efficiency of the truncated SVD representation are investigated, from both mathematical and experimental standpoints. Second, the question of the impact of the approximate truncated SVD on the accuracy of the forward problem is addressed. Third, the effect of the approximation on the performance the MR-CSI inversion technique is investigated.

Finally, let us mention that the truncated SVD is a well known regularization technique applicable to linear inverse problems [21]. In order to avoid any possible confusion, we underline here that it is both in a different context and with a different goal that we propose to use the truncated SVD: our direct problem

Manuscript received April 27, 2009; revised April 22, 2010; accepted May 25, 2010. Date of publication September 23, 2010; date of current version November 30, 2010. This work was supported in part by the National Sciences and Engineering Research Council of Canada (NSERC) Ph.D. and Postdoctoral Grants, Fonds québécois de la recherche sur la nature et les technologies (FQRNT) Ph.D. Grant, ANR-OPTIMED, FQNRT Grant #PR-113254, and in part by the NSERC Discovery Grant #138417-06.

P.-A. Barrière was with Department of Electrical Engineering, École Polytechnique de Montréal, Succ. Centre-ville Montréal, QC H3C 3A7, Canada, the Institut de Recherche en Communications et en Cybernétique de Nantes (IRCCyN), 44321 Nantes Cedex 03, France, and the Department of Information and Communication Technologies, University of Trent, I-38050 Trent, Italy (e-mail: paul-andre.barriere@polymtl).

J. Idier is with Institut de Recherche en Communications et en Cybernétique de Nantes (IRCCyN), 44321 Nantes Cedex 03, France (e-mail: Jerome.Idier@irccyn.ec-nantes.fr).

Yves Goussard and Jean-Jacques Laurin are with Department of Electrical Engineering, École Polytechnique de Montréal, Succ. Centre-ville Montréal, QC H3C 3A7, Canada (e-mail:yves.goussard@polymtl.ca; jean-jacques.laurin@polymtl.ca).

Digital Object Identifier 10.1109/TAP.2010.2078440

is nonlinear with respect to the quantity of interest, which is the contrast of electrical properties, and our aim is to reduce the computational burden to get a nearly unaltered solution.

II. Background

In a microwave tomography experiment, an object under test is placed within a domain D and is sequentially illuminated by M different microwave emitters. For each illumination, the scattered field is gathered at N points. By using the method of moment as a discretization technique, the microwave tomography experiment can be formulated as [12]:

for $i = 1, \ldots, M$

$$\boldsymbol{y}_i = \mathbf{G}_{\mathrm{o}} \boldsymbol{w}_i + \boldsymbol{n}_i^{\mathrm{o}} \tag{1a}$$

$$\boldsymbol{w}_i = \mathbf{X}(\boldsymbol{E}_i^0 + \mathbf{G}_{\mathrm{c}} \boldsymbol{w}_i) \tag{1b}$$

where bold-italic fonts and bold-straight fonts denote column vectors and matrices, respectively. $\boldsymbol{y}_i$ is a length-N vector that contains the measured scattered field related to the ith illumination. $\boldsymbol{E}_i^0$ is the incident field in D (i.e., the field when D is completely filled with the background medium). Its length is the number of discretization points, denoted by n. $\mathbf{G}_{\mathrm{o}}$ and $\mathbf{G}_{\mathrm{c}}$ are Green's matrices of size $N \times n$ and $n \times n$, respectively. $\mathbf{X}$ is a diagonal matrix such that $\mathbf{X} = \mathrm{diag}\{\boldsymbol{x}\}$. $\boldsymbol{x}$ and $\boldsymbol{w}_i$ are length-n vectors respectively referred to as the contrast vector and the current vector. Finally, $\boldsymbol{n}_i^{\mathrm{o}}$ is a noise vector that models all perturbations encountered in a microwave tomography experiment.

The unknown quantities are $\boldsymbol{x}$ and $\mathbf{W} = (\boldsymbol{w}_1, \ldots, \boldsymbol{w}_M)$; $\boldsymbol{x}$ represents the actual quantity of interest, since it contains all relevant information about the permittivity and conductivity of the object under test [12].

III. SVD Based Approximation

MR-CSI, which is detailed in Section IV.A, is based on (1a) and (1b). In the general case, the most expensive operations of the method are the matrix-vector products involving matrix $\mathbf{G}_{\mathrm{c}}$. Indeed, this matrix is large $(n \times n)$ and full (i.e., non-sparse). However, if the background medium is homogeneous and a uniform discretization grid is used, $\mathbf{G}_{\mathrm{c}}$ has a Toeplitz-block-Toeplitz (TBT) structure. In such a case, the matrix $\mathbf{G}_{\mathrm{c}}$ does not have to be explicitly built and the computation cost of a multiplication involving it can be reduced from $O(n^2)$ to $O(n \log n)$ by using a fast-Fourier-transform (FFT) algorithm [4]. Nevertheless, multiplications involving $\mathbf{G}_{\mathrm{c}}$ remain costly compared to other operations and such a strategy can only be used in some particular cases. In this paper we suggest to use an approximate form of $\mathbf{G}_{\mathrm{c}}$, based on its SVD, in order to accelerate the inversion process.

A. Truncated SVD of $\mathbf{G}_{\mathrm{c}}$

$\mathbf{G}_{\mathrm{c}}$ admits the following singular value decomposition

$$\mathbf{G}_{\mathrm{c}} = \mathbf{U} \boldsymbol{\Psi} \mathbf{V}^{\dagger} \tag{2}$$

where

$$\mathbf{U} = (\boldsymbol{u}_1, \ldots, \boldsymbol{u}_n) \tag{3a}$$

$$\mathbf{V} = (\boldsymbol{v}_1, \ldots, \boldsymbol{v}_n) \tag{3b}$$

$$\boldsymbol{\Psi} = \mathrm{diag}\{\boldsymbol{\psi}\} \tag{3c}$$

$$\boldsymbol{\psi} = (\psi_1, \ldots, \psi_n)^{\mathrm{T}}, \quad \psi_1 \geq \cdots \geq \psi_n \geq 0 \tag{3d}$$

and where $\cdot^{\dagger}$ and $\cdot^{\mathrm{T}}$ represent the transpose conjugate and transpose operations, respectively. Note that matrices $\mathbf{U}$ and $\mathbf{V}$ are square with size $n \times n$.

Our objective is to approximate $\mathbf{G}_{\mathrm{c}}$ by its truncated SVD (TSVD). More precisely, we define $\tilde{\mathbf{G}}_{\mathrm{c}}$, the approximation of $\mathbf{G}_{\mathrm{c}}$, as

$$\tilde{\mathbf{G}}_{\mathrm{c}} = \tilde{\mathbf{U}}_{\Psi} \tilde{\mathbf{V}}^{\dagger} \approx \mathbf{G}_{\mathrm{c}} \tag{4}$$

where

$$\tilde{\mathbf{U}}_{\Psi} = \tilde{\mathbf{U}} \tilde{\boldsymbol{\Psi}} \tag{5a}$$

$$\tilde{\mathbf{U}} = (\boldsymbol{u}_1, \ldots, \boldsymbol{u}_P) \tag{5b}$$

$$\tilde{\mathbf{V}} = (\boldsymbol{v}_1, \ldots, \boldsymbol{v}_P) \tag{5c}$$

$$\tilde{\boldsymbol{\Psi}} = \mathrm{diag}\{\tilde{\boldsymbol{\psi}}\} \tag{5d}$$

$$\tilde{\boldsymbol{\psi}} = (\psi_1, \ldots, \psi_P)^{\mathrm{T}}, \psi_1 \geq \psi_2 \geq \cdots \geq \psi_P. \tag{5e}$$

and where the value of P, which is smaller than n, is given by a truncating rule to be defined. Note that the $n \times n$ matrix $\mathbf{G}_{\mathrm{c}}$ is approximate by the product of two smaller matrices of size $n \times P$.

Obviously, such an approximation is possible only if

$$\psi_p \approx 0 \quad \forall p > P \tag{6}$$

i.e., if the singular values ψ_p decrease toward 0 (or toward a small value) when p increases. Moreover, from a computation point of view, the approximation will be efficient only if the decay of the singular values is relatively fast, i.e., if P is small with respect to n. In the next subsection we introduce results showing that the values of ψ_p actually converge systematically toward 0 and we quantify this decay.

B. Behavior of ψ_p

In [22], [23], the SVD of the operator linking the equivalents currents to the measured scattered field is analyzed and, on the basis of the fast decay of the singular values of the operator, conclusions are drawn in terms of degrees of freedom of the problem. However, these results cannot be directly applied to the problem at hand, as $\mathbf{G}_{\mathrm{c}}$ represents a different operator linking the same equivalent currents to the scattered field inside the reconstruction domain. Since the kernel of $\mathbf{G}_{\mathrm{c}}$ presents a singularity, different theoretical tools must be used.

Here, we first perform an analysis of the continuous operator, called $\mathcal{G}$, from which $\mathbf{G}_{\mathrm{c}}$ is derived. In this work, the analysis is limited to a 2D TM configuration [12] with a homogeneous background medium.

The product $\mathbf{G}_c \boldsymbol{w}_i$ is the discretized form of the following operation:

$$\mathcal{E}^s(x) = \int_{x' \in D} \tilde{g}_c(x, x') \mathcal{W}(x') dx' = \mathcal{G}\mathcal{W}(x) \qquad (7)$$

where $x \in D$. $\mathcal{E}^s$ and $\mathcal{W}$ are the continuous representations of the scattered field and of the currents, respectively and $\tilde{g}_c$ is the kernel of the integral operator. In our case, (7) represents a convolution operation with $\tilde{g}_c(x, x') = g_c(|x - x'|)$, where $g_c(\rho)$ is the zeroth order Hankel function of the second kind times a constant (i.e., the Green's function of the background medium) [12].

It is known that an integral operator is compact if its kernel is square-integrable [24], and that compact continuous operators admit a SVD with singular values that accumulate to zero [24]. It is shown in Appendix A that $\tilde{g}_c(x, x')$, with $x \in D$ and $x' \in D$, is square-integrable despite its singularity at $x = x'$. Therefore, operator $\mathcal{G}$ admits a SVD and has singular values which decay toward zeros. We now focus on the rate at which the decay occurs.

In [22], it is stated that the singular values of operators having an analytic kernel decrease to zero in a step-like fashion and with an exponential decay after the "knees". Unfortunately, in our case, the operator is not analytic due to the singularity mentioned above. Therefore, fast decay of the singular values can not be proven on such a basis. However, results showing that the singular values of a truncated convolution operator such as $\mathcal{G}$ may be asymptotically (i.e., as the size of D grows) approximated by the spectrum of the convolution kernel have been established, in both continuous [25] and discrete [26], [27] frameworks. Conditions sufficient for these results to hold include (*i*) the hermitian symmetry of the convolution kernel and (*ii*) the continuity of the spectrum of the convolution kernel. Here, condition (*i*) is not met since $\tilde{g}_c(x, x')$ is merely symmetric as opposed to hermitian. However, as noted in [25], the asymptotic approximation result holds in this case when one substitutes the singular values of the operator for its eigenvalues, and the modulus of the spectrum of the convolution kernel for its spectrum, respectively. Condition (*ii*) is not met either, essentially because of the slow decay of $g_c(\rho)$ when ρ goes to infinity. Nonetheless, the above results suggest that useful indications about the behavior of the singular values of $\mathcal{G}$ may be provided by the modulus of the Fourier transform of the truncated convolution kernel, or by discrete versions thereof since the analytic expression of the spectrum of $g_c(x)$ is known and decreases to zero fast when x increases. We now present numerical experiments which support this claim.

Let us first define $\mathbf{g}_t$ as the truncated version of the discrete convolution kernel. Fig. 1 compares the behavior of ψ_p with the one of $|\mathrm{DFT}(\mathbf{g}_t)|$ (after rearranging these quantities in decreasing order) for different configurations. Three different sizes of reconstruction domains and three different discretization steps were tested. More precisely, Fig. 1 (a)–(c) were obtained with a unique discretization step of $\lambda_0/20$, where λ_0 is the wavelength in the background medium, and with domains having side lengths of λ_0, $1.5\lambda_0$ and $2\lambda_0$, respectively. Fig. 1 (d) and (e) were obtained with a unique domain D with

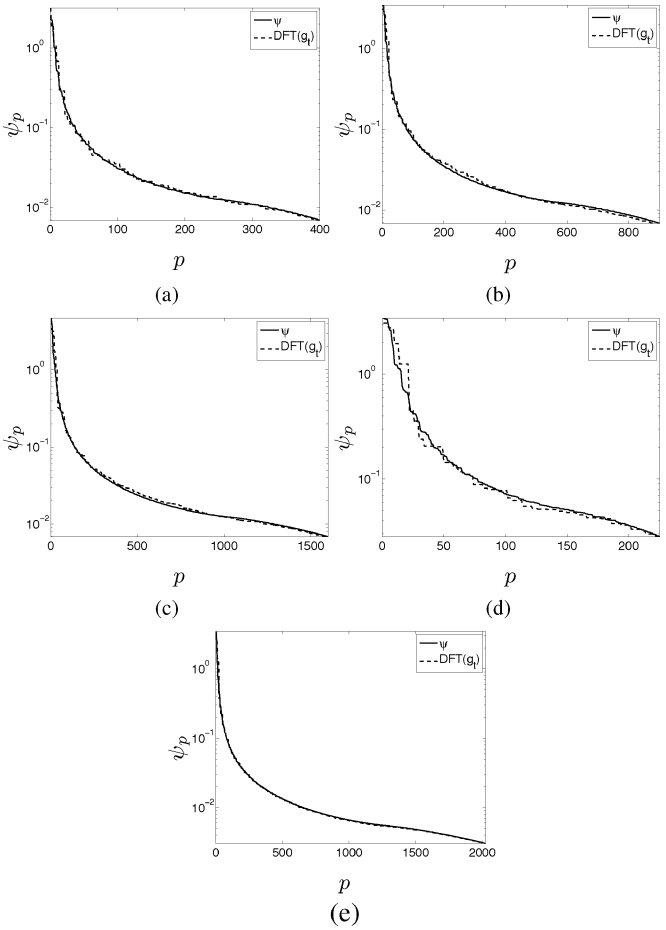

Fig. 1. Comparison of ψ_p with $|\mathrm{DTF}(\mathbf{g}_t)|$ for different sizes of domain ($A \times A$) and different discretization steps (Δ). Both quantities are sorted in a decreasing order. (a) $A = \lambda_0$, $\Delta = \lambda_0/20$, (b) $A = 1.5\lambda_0$, $\Delta = \lambda_0/20$, (c) $A = 2\lambda_0$, $\Delta = \lambda_0/20$, (d) $A = 1.5\lambda_0$, $\Delta = \lambda_0/10$, (e) $A = 1.5\lambda_0$, $\Delta = \lambda_0/30$.

side-length equal to $1.5\lambda_0$ and discretization steps equal to $\lambda_0/10$ and $\lambda_0/30$, respectively.

Three conclusions can be drawn from the examination of these results: (*i*) In all cases, the singular values ψ_p decrease toward zero. (*ii*) The decrease of ψ_p follows the one of $|\mathrm{DFT}(\mathbf{g}_t)|$ very closely. (*iii*) The rate of decay is quite fast, particularly for small values of p.

Both conditions for $\tilde{\mathbf{G}}_c$ to be a good and efficient approximation of $\mathbf{G}_c$, which are stated at the end of the previous subsection, are then met. In other words, the previous results suggest that $\tilde{\mathbf{G}}_c$ can be a very good approximation of $\mathbf{G}_c$ even for small values of P, i.e., even if only a few singular values of $\mathbf{G}_c$ are kept in the approximation. However, contrarily to cases reported in [22], the decrease does not occur in a step-like fashion. Then, there is no "obvious" choice for the truncating rule and different choices yield different trade-offs between truncating ratio and precision. Two different truncating rules are proposed in Section V.

Finally, let us me mentioned that, despite the fact that this analysis and the cases tested in this paper are limited to the homogeneous background scenario, we observed the same behavior for the values of ψ_p related to inhomogeneous backgrounds, like the one presented in [28]. Note that, in these cases,

the values of ψ_p cannot be compared to $|\mathrm{DFT}(\mathbf{g}_\mathrm{t})|$ since $\mathbf{g}_\mathrm{t}$ is undefined.

C. Truncated-$\mathbf{G}_\mathrm{c}$ Formulation

Before introducing how the proposed approximation can be used in an inversion algorithm, let us underline that this approximation can be used to form a new formulation of the microwave tomography problem in which (1a) remains unchanged and (1b) is replaced by

$$\boldsymbol{w}_i = \mathbf{X}\left(\boldsymbol{E}_i^0 + \tilde{\mathbf{U}}_\Psi \tilde{\mathbf{V}}^\dagger \boldsymbol{w}_i\right) + \tilde{\boldsymbol{n}}_i^c \tag{8}$$

where $\tilde{\boldsymbol{n}}_i^c$ models the errors due to approximation (6). According to the previous results, if P is correctly chosen, $\tilde{\boldsymbol{n}}_i^c$ should be small. Equations (1a) and (8) will be referred to as the truncated-$\mathbf{G}_\mathrm{c}$ formulation.

Note that the proposed approximation does not directly affect the contrast $\boldsymbol{x}$, which is the quantity of interest during the inversion process. Indeed, the product $\mathbf{G}_\mathrm{c}\boldsymbol{w}_i$ computes the scattered field inside domain D. Thus, only this field is approximated in our formulation, and the approximation can be made as good as one may want by increasing the value of P toward n.

IV. Application to the Inverse Problem

In this section, we apply the proposed approximation to an inverse scattering method: the MR-CSI algorithm. Let us first briefly introduce the MR-CSI approach before explaining how it can be adapted to the truncated-$\mathbf{G}_\mathrm{c}$ formulation.

A. MR-CSI

MR-CSI is an iterative method based on (1). At each iteration k, currents $\mathbf{W}$ and contrast $\boldsymbol{x}$ are alternately updated by minimizing the following criterion:

$$F^k(\boldsymbol{x}, \mathbf{W}) = \left(F_1 + F_2^k\right) F_\mathrm{r}^k \tag{9}$$

where

$$F_1 = \frac{\sum_i \|\boldsymbol{y}_i - \mathbf{G}_\mathrm{o}\boldsymbol{w}_i\|^2}{\sum_i \|\boldsymbol{y}_i\|^2} \tag{10a}$$

$$F_2^k = \frac{\sum_i \left\|\mathbf{X}\left(\boldsymbol{E}_i^0 + \mathbf{G}_\mathrm{c}\boldsymbol{w}_i\right) - \boldsymbol{w}_i\right\|^2}{\sum_i \left\|\mathbf{X}^{k-1}\boldsymbol{E}_i^0\right\|^2} \tag{10b}$$

$$F_\mathrm{r}^k = \int_D \frac{|\nabla \boldsymbol{x}|^2 + \delta_k^2}{V\left[|\nabla \boldsymbol{x}^{k-1}|^2 + \delta_k^2\right]} dv \tag{10c}$$

V is the volume of D and

$$\delta_k^2 = \frac{\sum_i \left\|\mathbf{X}^{k-1}\left(\boldsymbol{E}_i^0 + \mathbf{G}_\mathrm{c}\boldsymbol{w}_i^k\right) - \boldsymbol{w}_i^k\right\|^2}{\sum_i \left\|\mathbf{X}^{k-1}\boldsymbol{E}_i^0\right\|^2} \tilde{\Delta}^2 \tag{11}$$

where $\tilde{\Delta}^2$ denotes the reciprocal mesh size of the discretized domain D [13].

More details about MR-CSI, the procedure used to update $\boldsymbol{x}$ and $\mathbf{W}$ and the stopping rules can be found in [13], [14].

B. MR-CSI Based on the Truncated-$\mathbf{G}_\mathrm{c}$ Formulation

We propose to use the truncated-$\mathbf{G}_\mathrm{c}$ formulation with the MR-CSI method. More precisely, we suggest to replace $\mathbf{G}_\mathrm{c}$ by $\tilde{\mathbf{U}}_\Psi \tilde{\mathbf{V}}^\dagger$ in (10b) and (11). Since the resulting criterion has the same form as the original one, the minimization algorithm of the MR-CSI method can be used with the only difference that each product by $\mathbf{G}_\mathrm{c}$ is replaced by two products with a total elementary multiplication count of $2Pn$. By using the truncated-$\mathbf{G}_\mathrm{c}$ formulation with the MR-CSI approach, one can then expect to significantly accelerate the inversion process (since $P \ll n$) without significantly altering the solution (since $\tilde{\mathbf{G}}_\mathrm{c} \approx \mathbf{G}_\mathrm{c}$). Before validating this hypothesis with experimental results, we address the question related to the computation cost of the SVD of $\mathbf{G}_\mathrm{c}$.

C. SVD Computation Cost

The computation cost of a singular value decomposition raises extremely rapidly with the size of the problem. One can then question the benefit of using the proposed approach for very large problems.

A salient feature of the truncated-$\mathbf{G}_\mathrm{c}$ formulation is that the SVD has to be calculated only once for a given configuration. Therefore, large computation times may be acceptable. Moreover, algorithms capable of performing truncated SVD, i.e., capable of computing only the first Q singular values and vectors of a matrix, are available. This produces a significant decrease in the computation costs since only few singular values are needed in our formulation. Nevertheless, this approach may not be sufficient for very large problems.

The computation of singular values and vectors has been studied extensively and a number of algorithms are available. It is not the aim of this paper to compare or analyze them. However, from a practical standpoint, we observed that, for all configurations used in this paper, the maximal time for the SVD computation was 83 seconds (for a case where $n = 40^2 = 1600$) and the minimal one was 4 seconds (for a case where $n = 20^2 = 400$). Computations were performed on a PC running Windows Server 2008 and configured with a quad-core processor clocked at 3 GHz and 12 GB of RAM. We used the `svds` function of Matlab 7.5 to perform the SVD.

V. Results

In this section the efficiency of the truncated-$\mathbf{G}_\mathrm{c}$ formulation is validated. We first compare the solutions of the forward problem obtained with and without the approximation. Then the impact of the proposed formulation on the solutions provided by the MR-CSI method is analyzed. Two truncating rules, leading to different trade-offs between computation cost and solution quality, are proposed.

Tests were performed on both synthetic and experimental data and were limited to the 2-D TM case [12] with a homogeneous background medium. For synthetic data, two reconstruction domains were considered. Both were square with side length A of

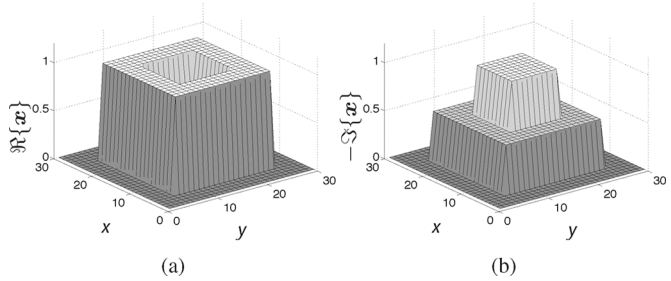

Fig. 2. (a) Real and (b) opposite value of the imaginary parts of the contrast of the *square cylinder object* in domain 1. The x and y axes are indexed by the sample number.

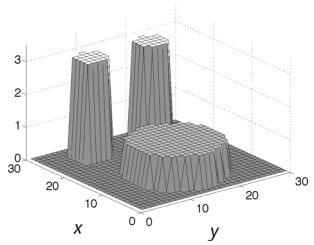

Fig. 3. Real part of the contrast of the Ö *object* in domain 1. The imaginary part is set to zero. The x and y axes are indexed by the sample number.

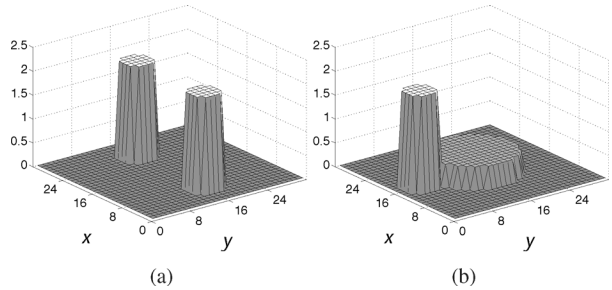

Fig. 4. Real parts of the contrasts of (a) the *homogeneous object* [32] and (b) *inhomogeneous object* [33]. Both objects have a purely real contrast.

$1.5\lambda_0$ for the first domain and $2\lambda_0$ for the second one. We will refer to them as domains 1 and 2, respectively. The same discretization step of $\lambda_0/20$ was used in both cases.[1] The number of discretization points was $n = 30^2 = 900$ for domain 1 and $n = 40^2 = 1600$ for domain 2. In each case, we used $M = N = 30$ with emitters and receivers equally spaced on a circle with radius $1.01A/\sqrt{2}$ whose center coincided with the center of D. Experiments were limited to single frequency harmonic excitation.

For each reconstruction domain, two objects under test were considered. The contrast distributions of both objects tested in domain 1 are shown in Figs. 2 and 3. We will refer to them as the *square cylinder* and Ö objects, respectively. The *square cylinder object* was made of two concentric square cylinders; the contrast values for the outer and inner cylinders were $1-0.5j$ and $0.5-j$, respectively. The Ö *object* was made of three circular cylinders placed in an O fashion (this contrast distribution was inspired by [31]). The contrast of the cylinders was constant and purely real with a value of 1 for the large cylinder and 3 for the two small ones. For domain 2, the same two objects were tested but their dimensions were scaled in proportion to the size of the domain.

[1]We assumed that the range of the contrast values to be rebuilt was between 0 and 3. We used a discretization step equal to one tenth of the wavelength in the highest permittivity material, which leads to a discretization step of $\lambda_0/20$. Such a choice is frequently done and inspired by the works of Richmond [29], [30].

TABLE I
SUMMARY OF THE TESTED CONFIGURATIONS. * INDICATES THAT THE OBJECT DIMENSIONS WERE SCALED IN PROPORTION TO THE RECONSTRUCTION DOMAIN

	Domain size	Discr. points	Tested objects
Synth. data	$1.5\lambda_0 \times 1.5\lambda_0$ (name: domain 1)	$n = 30^2 = 900$	*square cyl.* Ö
	$2\lambda_0 \times 2\lambda_0$ (name: domain 2)	$n = 40^2 = 1600$	*square cyl.** Ö*
Exp. data	$1.6\lambda_0 \times 1.6\lambda_0$	$n = 32^2 = 1024$	*homogen. inhomogen.*

We also used experimental data from the Fresnel Institute[2] databases. Tests were performed with the 3 GHz dataset of the experiments reported in [32] and [33] for quasi 2-D setups. Here we present results obtained with two of the tested objects. The real parts of their contrasts are shown in Fig. 4. For both objects, the imaginary part was equal to zero (i.e., lossless objects). We will refer to the object presented in Fig. 4(a) as the *homogeneous object* [32] while the object presented in Fig. 4(b) will be referred to as the *inhomogeneous object* [33]. In both cases, we used a reconstruction domain of $1.6\lambda_0 \times 1.6\lambda_0$ and a discretization step of $\lambda_0/20$, which leads to $n = 32^2 = 1024$. The number of emitters (M) and receivers (N) used for the experiments at the Fresnel Institute were $M = 36, N = 49$ for the *homogeneous object* and $M = 8, N = 241$ for the *inhomogeneous object*. The receivers were distributed on a circle whose center coincided with the center of D. The radius of this circle was 0.76 m $(7.6\lambda_0)$ for the *homogeneous object* and 1.67 m $(16.7\lambda_0)$ for the *inhomogeneous* one. The different configurations are summarized in Table I.

A. Forward Problem

First, we solved the forward problem for the synthetic cases with both classical and approximated formulations and we compared the resulting scattered fields at the receiver level. In other words, we compared the quantities

$$\boldsymbol{y}_i^s = \mathbf{G}_{\mathrm{o}}(\mathbf{I} - \mathbf{X}\mathbf{G}_{\mathrm{c}})^{-1}\mathbf{X}\boldsymbol{E}_i^0 \tag{12}$$

and

$$\tilde{\boldsymbol{y}}_i^s = \mathbf{G}_{\mathrm{o}}(\mathbf{I} - \mathbf{X}\hat{\mathbf{U}}_\Psi\hat{\mathbf{V}}^\dagger)^{-1}\mathbf{X}\boldsymbol{E}_i^0. \tag{13}$$

Quantitative assessment of the quality of the truncated-$\mathbf{G}_{\mathrm{c}}$ formulation was performed using the relative mean square error defined as

$$\Delta_{\boldsymbol{y}} = \frac{\sum_{i=1}^{M} \|\tilde{\boldsymbol{y}}_i^s - \boldsymbol{y}_i^s\|^2}{\sum_{i=1}^{M} \|\boldsymbol{y}_i^s\|^2}. \tag{14}$$

We tested two different SVD truncating rules respectively referred to as P_1 and P_2. P_1 is defined as the smallest index p such that $\psi_p < \psi_1/20$ while $P_2 \stackrel{\triangle}{=} 2\ P_1$. Table II gives the

[2]Fresnel Institute—Marseille: http://www.fresnel.fr.

TABLE II
VALUES OF P_1 AND P_2 FOR DOMAINS 1 AND 2 AND ASSOCIATED PERCENTAGE OF TRUNCATED SINGULAR VALUES

	P_1	Trunc. sing. values	P_2	Trunc. sing. values
Domain 1	51	94%	102	89%
Domain 2	67	96%	134	91%

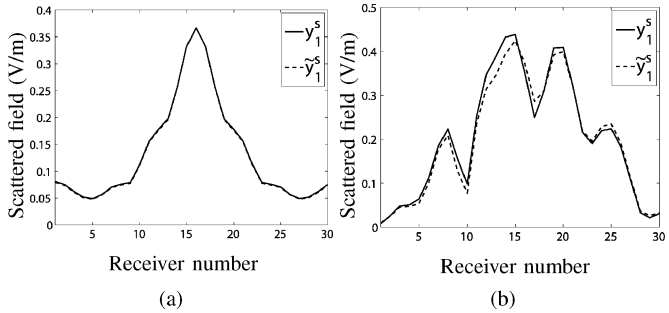

Fig. 5. Amplitude of the expected measured scattered field for the classical formulation ($\boldsymbol{y}_1^s$) and for the truncated-$\mathbf{G}_c$ formulation ($\tilde{\boldsymbol{y}}_1^s$), (a) *square cylinder object* and (b) Ö *object*. $P = P_1$. Domain 1 was used.

TABLE III
$\Delta_{\boldsymbol{y}}$ FOR BOTH VALUES OF P AND FOR ALL SYNTHETIC TEST CASES

	square cylinder object	
	P_1	P_2
Dom. 1	1.1×10^{-4} (-40 dB)	2.2×10^{-6} (-57 dB)
Dom. 2	3.3×10^{-4} (-35 dB)	1.0×10^{-5} (-50 dB)
	Ö *object*	
	P_1	P_2
Dom. 1	1.7×10^{-2} (-18 dB)	8.2×10^{-4} (-31 dB)
Dom. 2	6.0×10^{-2} (-12 dB)	8.1×10^{-4} (-31 dB)

exact values of P_1 and P_2 for domains 1 and 2 as well as the percentage of truncated singular values related to these choices. It can be observed that this ratio increases with the size of the domain.

The mean square error values ($\Delta_{\boldsymbol{y}}$) obtained for both values of P and for all synthetic test cases are reported in Table III. Fig. 5 also depicts the quantities $|\boldsymbol{y}_1^s|$ and $|\tilde{\boldsymbol{y}}_1^s|$ for both objects in domain 1 with $P = P_1$.

As a general rule, we observe that the mean square errors generally increase with the size of the object and with the contrast value. However, in most cases, the MSEs remain very low. More precisely, MSE values obtained with the *square cylinder object* are very small (below -35 dB) for both values of P and for both domain sizes. For the Ö *object*, MSEs are also very small (below -30 dB) when P_2 is used while, when P_1 is used, they are significantly higher. According to these results, we conclude that the proposed approximation leads to almost no loss of information when P_2 is used, and thus despite the fact that more than 89% of the singular values of $\mathbf{G}_c$ are not used in the formulation. When P_1 is used, this percentage increases to at least 94% and it seems that there is still almost no loss of information for objects having relatively small dimensions or low contrast values.

TABLE IV
RECONSTRUCTION TIMES AND MEAN SQUARE ERRORS OBTAINED FOR SYNTHETIC OBJECTS WITH BOTH FORMULATIONS

		Computation time (s)				Δ_x		
		Class. form.		Trunc.-$\mathbf{G}_c$		Class.	Trunc.-$\mathbf{G}_c$	
		FFT	No FFT	P_1	P_2	form.	P_1	P_2
Dom. 1	Square. cyl.	32	63	17	21	0.04	0.04	0.04
	Ö obj.	27	52	14	17	0.11	0.09	0.11
Dom. 2	Square. cyl.	146	190	32	42	0.05	0.06	0.04
	Ö obj.	147	191	31	42	0.08	0.13	0.09

TABLE V
RECONSTRUCTION TIMES AND MEAN SQUARE ERRORS OBTAINED FOR OBJECTS OF THE FRESNEL INSTITUTE WITH BOTH FORMULATIONS

	Computation time (s)				Δ_x		
	Class. form.		Trunc.-$\mathbf{G}_c$		Class.	Trunc.-$\mathbf{G}_c$	
	FFT	No FFT	P_1	P_2	form.	P_1	P_2
Homog. object	50	67	22	27	0.47	0.48	0.47
Inhomog. object	16	34	13	15	0.13	0.14	0.13

We now study the impact of our formulation on the inversion process.

B. Inverse Problem

We applied the truncated-$\mathbf{G}_c$ formulation to the MR-CSI method. Once again, quantitative assessment of the quality of the solution was performed using the relative mean square error defined as

$$\Delta_{\boldsymbol{x}} = \|\boldsymbol{x} - \boldsymbol{x}_o\|^2 / \|\boldsymbol{x}_o\|^2 \tag{15}$$

where $\boldsymbol{x}_o$ is the actual contrast. Note that white Gaussian noise was added to each set of simulated data in order to get a 20 dB signal-to-noise ratio.

For each object, solutions were computed in four cases: (*i*) classical formulation, FFT used to accelerate matrix-vector products involving $\mathbf{G}_c$, (*ii*) classical formulation, FFT *not* used to accelerate matrix-vector products involving $\mathbf{G}_c$, (*iii*) truncated-$\mathbf{G}_c$ formulation, $P = P_1$, (*iv*) truncated-$\mathbf{G}_c$ formulation, $P = P_2$. Both the computation time and the mean square error were compared (obviously, the mean square error values were the same in cases 1 and 2). We underline that, for a given configuration, i.e., a given object and a given reconstruction domain, the same number of iterations was performed with all formulations.

Tables IV and V summarize the results for the synthetic and experimental cases, respectively. The reconstructions are presented in Figs. 6 to 9 (for synthetic cases, only the results obtained with domain 1 are presented due to space considerations).

Comparison of the mean square errors suggest that the solutions provided by classical and truncated-$\mathbf{G}_c$ formulations are equivalent in all cases when P_2 is used. This is confirmed by

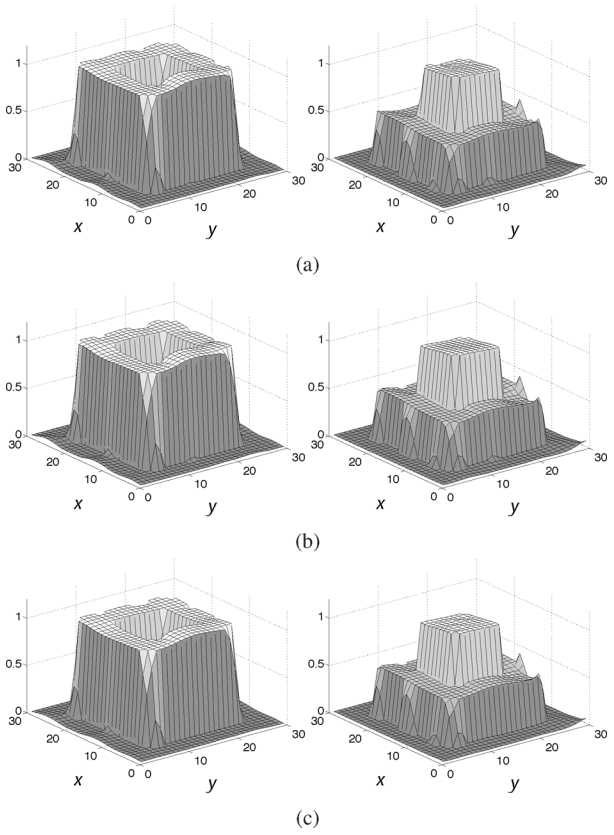

Fig. 6. Reconstructions of the *square cylinder object* in domain 1. Real part on the left side, opposite value of the imaginary part on the right one. (a) Truncated-$\mathbf{G}_c$ formulation with $P = P_1$, (b) Truncated-$\mathbf{G}_c$ formulation with $P = P_2$, (c) classical formulation. The x and y axes are indexed by the sample number.

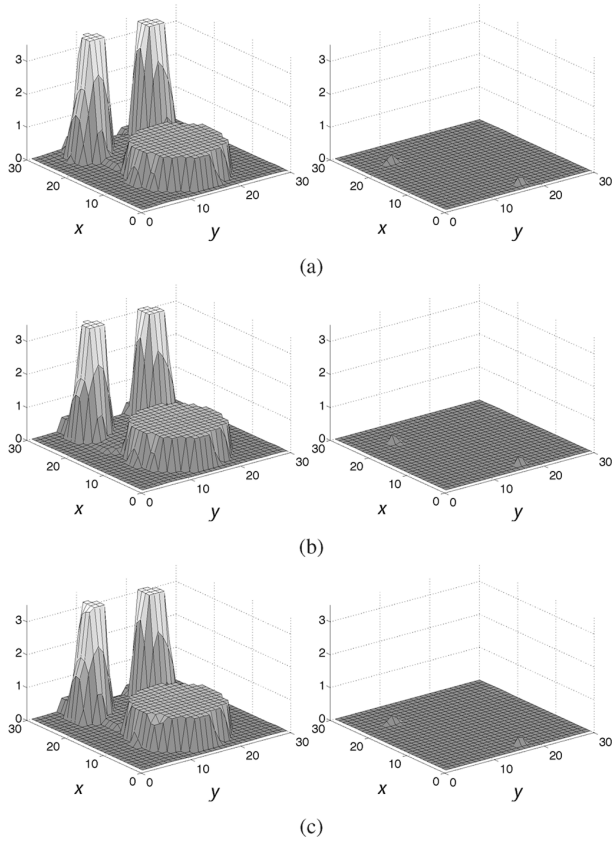

Fig. 7. Reconstructions of the Ö *object* in domain 1. (a) Truncated-$\mathbf{G}_c$ formulation with $P = P_1$, (b) truncated-$\mathbf{G}_c$ formulation with $P = P_2$, (c) classical formulation. Same type of representation as in Fig. 6.

comparing part (b) to part (c) in Figs. 6 to 9. Indeed, a qualitative examination shows that the solutions are almost identical in all cases. When P_1 is used, solutions equivalent to the ones of the classical formulation are also obtained with three of the four tested objects, i.e., with the *square cylinder*, *homogeneous* and *inhomogeneous* objects. This is confirmed both by the comparison of the MSE values and by the examination of Figs. 6 (a) and (c), 8 (a) and (c), and 9 (a) and (c). The Ö *object* with $P = P_1$ is the only case where the truncated-$\mathbf{G}_c$ and classical formulations do not produce equivalent solutions. This confirms that the truncated-$\mathbf{G}_c$ formulation looses precision when the contrast values increase (recall that the Ö *object* is the only one involving contrast values of 3). The worst case occurs for domain 2, where the MSE increases from 0.08 to 0.13 when the truncated-$\mathbf{G}_c$ formulation is used. However, inspection of the solutions obtained in this particular test case, presented in Fig. 10, shows that the reconstruction obtained with the proposed formulation is still very acceptable and that it is quite similar to the one given by the classical formulation. Moreover, for domain 1, the reconstruction obtained with the approximate formulation is better than the one obtained with the classical formulation. In summary, we can claim that solutions equivalent to the ones produced by the classical MR-CSI method are obtained if P_2 is used. If P_1 is used, equivalent solutions are also obtained for small objects or objects involving small contrast values while different but still acceptable solutions are obtained otherwise. All these results confirm the efficiency of the approximation regarding the quality of the solution.

The comparison of the computation times shows that the truncated-$\mathbf{G}_c$ formulation produces an acceleration of the inversion process in all cases. Moreover, in most of the cases, this acceleration is significant. More precisely, when P_1 is used, the computation time decreases by a factor ranging from 1.2 to 4.7 (average of 2.8) compared to the cases where the FFT is used while it decreases by a factor ranging from 2.6 to 6.2 (average of 4.2) otherwise. When P_2 is used, the computation time decreases by a factor ranging from 1.1 to 3.5 (average of 2.2) compared to the case where the FFT is used while it decreases by a factor ranging from 2.3 to 4.5 (average of 3.3) otherwise. Finally, using P_1 instead of P_2 yields an additional decrease of the computation time of approximately 25%.

Note that, when FFT is used with the classical formulation, the relative acceleration obtained with the proposed formulation varies significantly from one test case to the other. This is due to the fact that the FFT algorithm is optimal when the size of the discretized convolution kernel is a power of two (zero padding can be used to reach the nearest power of two but this leads to an artificial increase of the size of the problem). This explains why the time reduction obtained with the truncated-$\mathbf{G}_c$ formulation is less important when the domain size is 30×30 (domain 1)

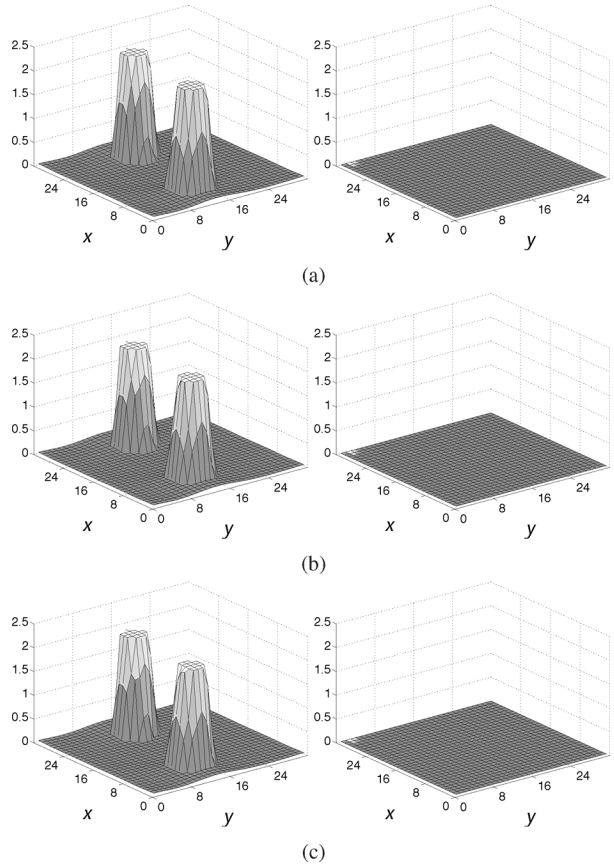

Fig. 8. Reconstructions of the *homogeneous object*. (a) Truncated-$\mathbf{G}_c$ formulation with $P = P_1$, (b) truncated-$\mathbf{G}_c$ formulation with $P = P_2$, (c) classical formulation. Same type of representation as in Fig. 6.

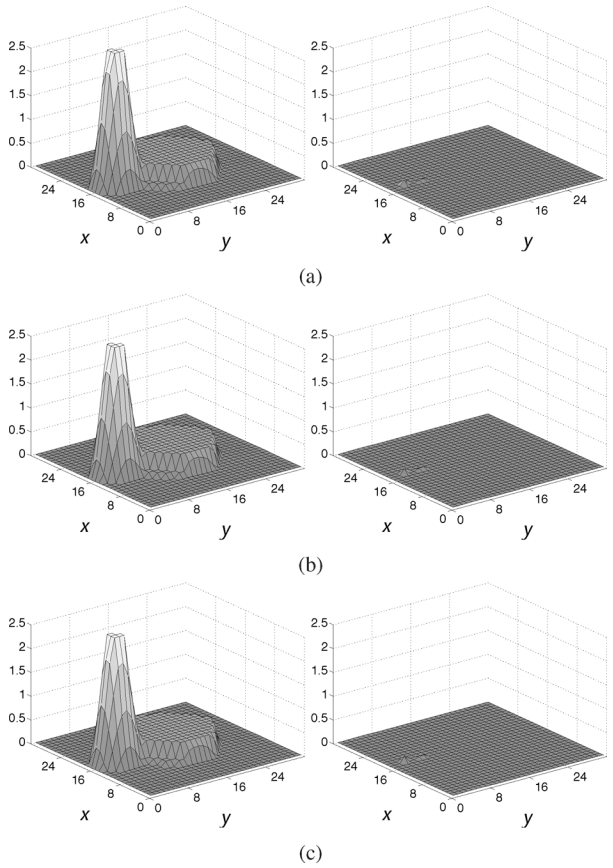

Fig. 9. Reconstruction of the *inhomogeneous object*. (a) Truncated-$\mathbf{G}_c$ formulation with $P = P_1$, (b) truncated-$\mathbf{G}_c$ formulation with $P = P_2$, (c) classical formulation. Same type of representation as in Fig. 6.

and 32×32 (experimental data) while it is maximal when the domain size is 40×40 (domain 2).

Finally, it can be observed that the time reductions were less important with the *inhomogeneous object*. This can be explained by the fact that, in this case, the number of data points (N) and thus the size of $\mathbf{G}_o$ were significantly larger than in other cases while the size of $\mathbf{G}_c$ remained unchanged. Therefore, the relative gain coming from the approximation of $\mathbf{G}_c$ was less important.

In any case, all these results confirm the efficiency of the proposed method. Moreover, they suggest that the choice between the two proposed truncating rules should be made according to the characteristics of the application at hand. Indeed, in applications involving mainly low contrasts and/or in applications where small reconstruction errors can be tolerated, the rule P_1 should be chosen since it leads to a maximal decrease of the computation time. In other cases, the rule P_2, which provides solutions equivalent to the ones of the classical formulation, should be preferred.

VI. Conclusion

This paper proposes an alternative approximate formulation of the microwave tomography problem which yields a significant reduction of the computation time of the MR-CSI algorithm. We based our work on the observation that the speed of this method is limited by the large size and the non-sparsity of the matrices involved in the microwave tomography equations.

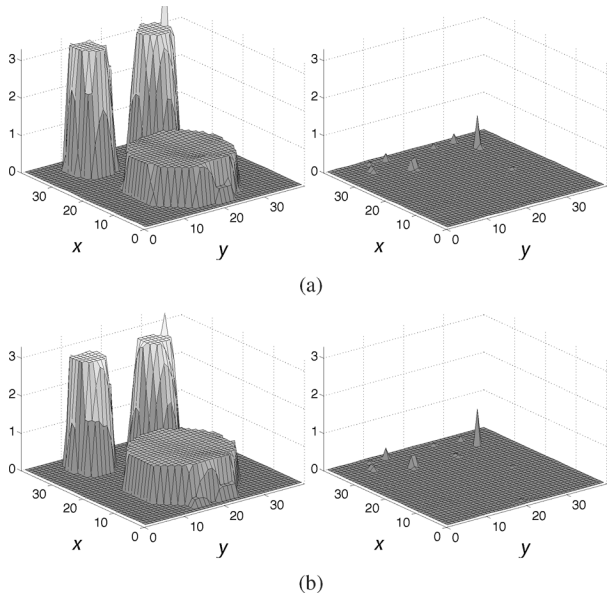

Fig. 10. Reconstruction of the Ö *object* in domain 2. Real part on the left side, opposite value of the imaginary part on the right one. (a) Truncated-$\mathbf{G}_c$ formulation with $P = P_1$, (b) classical formulation. The x and y axes are indexed by the sample number.

To overcome this problem we suggested to replace $\mathbf{G}_c$ by its truncated SVD. A study of the behavior of the singular values indicates that their values can be closely approximated by the DFT of a truncated version of the convolution kernel, and that their decay toward zero is quite fast. In addition, integration of the resulting truncated-$\mathbf{G}_c$ formulation into the MR-CSI algorithm is straightforward and results in a lower total computation cost.

Regarding truncation of the SVD, two rules were proposed. With one of them, the proposed formulation yielded solutions equivalent to those obtained with the classical formulation while approximately 90% of the singular values were not kept in the approximation. With the other one, approximately 95% of the singular values were removed and the solutions provided by the proposed formulation were equivalent (for low contrast or small objects) or quite close to the ones provided by the classical formulation. At the end, the computation times of the inverse problems were reduced by a factor ranging from 1.1 to 6.2 depending on the setup configuration and on the object under test. Finally note that the proposed technique can be directly applied for solving the forward scattering problem, and that similar computational savings should be expected.

APPENDIX

A. Proof That the Kernel of $\mathcal{G}$ is Square Integrable

The goal of this Appendix is to show that $\tilde{g}_c(x, x')$ is square integrable on $D \times D$. Let us define $\mathcal{I}$ as

$$\mathcal{I} = \int_{x\in D} \int_{x'\in D} |\tilde{g}_c(x, x')|^2 dx' dx \tag{16}$$

and the sets $T(x)$ and U as

$$T(x) = \{x - x', x' \in D\} \tag{17}$$

$$U = \bigcup_{x\in D} T(x) = \{x - x', x' \in D, x \in D\}. \tag{18}$$

Given that $\tilde{g}_c(x, x') = g_c(|x - x'|)$ we can write (16) as

$$\mathcal{I} = \int_{x\in D} \int_{t\in T(x)} |g_c(|t|)|^2 dt dx \tag{19}$$

and we can deduce the following inequality:

$$\mathcal{I} \leq \int_{x\in D} dx \int_{t\in U} |g_c(|t|)|^2 dt. \tag{20}$$

The right term of (20) is a product of two independent integral operations. The result of the first one ($\int_{x\in D} dx$) is finite since D is finite. The result of the second operation ($\int_{t\in U} |g_c(t)|^2 dt$) is also finite since D is finite and $|g_c|^2$ is integrable in the vicinity of its singularity (the proof is rather simple and omitted here). We then have that $\mathcal{I}$ is finite, hence the proof.

REFERENCES

[1] E. C. Fear, P. M. Meaney, and M. A. Stuchly, "Microwaves for breast cancer detection?," *IEEE Potentials*, vol. 22, no. 1, pp. 12–18, 2003.

[2] Y. Xie, B. Guo, L. Xu, J. Li, and P. Stoica, "Multistatic adaptative microwave imaging for early breast cancer detection," *IEEE Trans. Biomed. Eng.*, vol. 53, no. 8, pp. 1647–1657, 2006.

[3] P. M. Meaney, M. W. Fanning, D. Li, S. P. Poplack, and K. D. Paulsen, "A clinical prototype for active microwave imaging of the breast," *IEEE Trans. Microwave Theory Tech.*, vol. 48, no. 11, pp. 1841–1853, 2000.

[4] T. Isernia, V. Pascazio, and R. Pierri, "A nonlinear estimation method in tomographic imaging," *IEEE Trans. Geosci. Remote Sensing*, vol. 35, no. 4, pp. 910–922, 1997.

[5] W. C. Chew and Y. M. Wang, "Reconstruction of two-dimensional permittivity distribution using the distorted Born iterative method," *IEEE Trans. Medical Imaging*, vol. 9, no. 2, pp. 218–225, 1990.

[6] N. Joachimowicz, C. Pichot, and J.-P. Hugonin, "Inverse scattering: An iterative numerical method for electromagnetic imaging," *IEEE Trans. Antennas Propag.*, vol. 39, no. 12, pp. 1742–1752, 1991.

[7] A. Franchois and C. Pichot, "Microwave imaging—Complex permittivity reconstruction with a Levenberg-Marquardt method," *IEEE Trans. Antennas Propag.*, vol. 45, no. 2, pp. 203–215, 1997.

[8] T. Isernia, L. Crocco, and M. D'Urso, "New tools and series for scattering problems in lossy media," *IEEE Trans. Geosci. Remote Sensing Lett.*, vol. 1, no. 4, pp. 327–331, 2004.

[9] I. Catapano, L. Crocco, M. D'Urso, and T. Isernia, "3D microwave imaging via preliminary support reconstruction: Testing on the Fresnel 2008 database," *Inverse Prob.*, vol. 25, no. 2, p. 23, 2009.

[10] P. M. van den Berg, A. L. van Broekhoven, and A. Abubakar, "Extended contrast source inversion," *Inverse Prob.*, vol. 15, pp. 1325–1344, 1999.

[11] A. Abubakar and P. M. van den Berg, "Total variation as a multiplicative constraint for solving inverse problems," *IEEE Trans. Image Processing*, vol. 10, no. 9, pp. 1384–1392, 2001.

[12] A. Abubakar, P. M. van den Berg, and J. J. Mallorqui, "Imaging of biomedical data using a multiplicative regularized contrast source inversion method," *IEEE Trans. Microwave Theory Tech.*, vol. 50, no. 7, pp. 1761–1771, 2002.

[13] P. M. van den Berg, A. Abubakar, and J. T. Fokkema, "Multiplicative regularization for profile inversion," *Radio Sci.*, vol. 38, no. 2, pp. VIC23-1–10, 2003.

[14] A. Abubakar, P. M. van den Berg, and T. M. Habashy, "Application of the multiplicative regularized contrast source inversion method on TM- and TE-polarized experimental Fresnel data," *Inverse Prob.*, vol. 21, no. 6, pp. S5–S13, 2005.

[15] M. Li, A. Abubakar, and P. M. van den Berg, "Application of the multiplicative regularized contrast source inversion method on 3D experimental Fresnel data," *Inverse Prob.*, vol. 25, no. 2, p. 23, 2009.

[16] P. M. van den Berg and R. E. Kleinman, "A contrast source inversion method," *Inverse Prob.*, vol. 13, pp. 1607–1619, 1997.

[17] C. Yu, M. Yuan, J. Stang, E. Bresslour, R. T. George, G. A. Ybarra, W. T. Joines, and Q. H. Liu, "Active microwave imaging II: 3-D system prototype and image reconstruction from experimental data," *IEEE Trans. Microwave Theory Tech.*, vol. 56, no. 4, pp. 991–1000, 2008.

[18] B. Wei, E. Imek, C. Yu, and Q. H. Liu, "Three-dimensional electromagnetic nonlinear inversion in layered media by a hybrid diagonal tensor approximation: Stabilized biconjugate gradient fast Fourier transform method," *Waves Random Complex Media*, vol. 17, no. 2, pp. 129–147, 2007.

[19] I. Catapano, L. Crocco, and T. Isernia, "Improved sampling methods for shape reconstruction of 3-D buried targets," *IEEE Trans. Geosci. Remote Sensing*, vol. 46, no. 10, pp. 3265–3273, 2008.

[20] M. D'Urso, I. Catapano, L. Crocco, and T. Isernia, "Effective solution of 3-D scattering problems via series expansions: Applicability and a new hybrid scheme," *IEEE Trans. Geosci. Remote Sensing*, vol. 45, no. 3, pp. 639–648, 2007.

[21] M. Z. Nashed, "Operator-theoretic and computational approaches to ill-posed problems with applications to antenna theory," *IEEE Trans. Antennas Propag.*, vol. 29, pp. 220–231, 1981.

[22] O. M. Bucci and T. Isernia, "Electromagnetic inverse scattering: Retrievable information and measurements strategies," *Radio Sci.*, vol. 32, no. 6, pp. 2123–2197, 1997.

[23] O. M. Bucci and G. Franceschetti, "On the degrees of freedom of scattered fields," *IEEE Trans. Antennas Propag.*, vol. 37, no. 7, pp. 918–926, 1989.

[24] A. V. Balakrishnan, *Applied Functional Analysis*, 2nd ed. New York: Springer-Verlag, 1981.

[25] A. Bottcher, "Pseudospectra and singular values of large convolution operators," *J. Int. Equat. Applicat.*, vol. 6, no. 3, pp. 267–301, 1994.

[26] U. Grenander and G. Szegö, *Toeplitz Forms and Their Applications*. Berkeley: Univ. Calif. Press, 1958.
[27] P. A. Voois, "A theorem on the asymptotic eigenvalue distribution of Toeplitz-block-Toeplitz matrices," *IEEE Trans. Signal Processing*, vol. 44, no. 7, pp. 1837–1841, Jul. 1996.
[28] P.-A. Barrière, J.-J. Laurin, Y. Goussard, and J. Idier, "Microwave tomography for breast cancer detection based on dielectric waveguide excitation, preliminary study," in *Proc. 10th Workshop on Optimization and Inverse Prob. in Electromagnetism*, Ilmenau, Germany, Sep. 2008, pp. 77–78.
[29] J. Richmond, "Scattering by a dielectric cylinder of arbitrary cross section shape," *IEEE Trans. Antennas Propag.*, vol. 13, no. 3, pp. 334–341, 1965.
[30] J. Richmond, "TE-wave scattering by a dielectric cylinder of arbitrary cross-section shape," *IEEE Trans. Antennas Propag.*, vol. 14, no. 4, pp. 460–464, 1966.
[31] K. Belkebir and A. G. Tijhuis, "Using multiple frequency information in the iterative solution of a two-dimensional non-linear inverse problem," presented at the PIERS 96: Progress in Electromagnetic Research Symp., Innsbruck, Austria, 1996.
[32] K. Belkebir and M. Saillard, "Special section: Testing inversion algorithms against experimental data," *Inverse Prob.*, vol. 17, no. 6, pp. 1565–1571, 2001.
[33] J.-M. Geffrin, P. Sabouroux, and C. Eyraud, "Free space experimental scattering database continuation: Experimental set-up and measurement precision," *Inverse Prob.*, vol. 21, no. 6, pp. S117–S130, Dec. 2005.

Paul-André Barrière received the B.Eng. degree in electrical engineering from the Université Laval, Quebec City, Canada, in 2002, the M.A.Sc. degree in electrical engineering from the Ecole Polytechnique de Montréal, Canada, in 2004, and the Ph.D. degree in electrical engineering from the Ecole Polytechnique de Montréal and the Ecole Centrale de Nantes, France, in 2008.

From 2009 to 2010, he was a Postdoctoral Researcher at the ELEDIA Laboratory, Department of Information Engineering and Computer Science (DISI), University of Trent, Italy. His research interests include inverse problems in electromagnetism.

Jérôme Idier (M'91) was born in France in 1966. He received the Diploma degree in electrical engineering from École Supérieure d'Électricité, Gif-sur-Yvette, France, in 1988 and the Ph.D. degree in physics from the University of Paris-Sud, Orsay, France, in 1991.

In 1991, he joined the Centre National de la Recherche Scientifique. He is currently a Senior Researcher at the Institut de Recherche en Communications et Cybernétique in Nantes, France. His major scientific interests are in probabilistic approaches to inverse problems for signal and image processing.

Dr. Idier is serving as an Associate Editor for the IEEE TRANSACTIONS ON SIGNAL PROCESSING and for the *Journal of Electronic Imaging*.

Yves Goussard (M'90) was born in Paris, France, in 1957. He graduated from the École Nationale Supérieure de Techniques Avancées in 1980 and received the Docteur-Ingénieur and Ph.D. degrees from the Université de Paris-Sud, Orsay, France, in 1983 and 1989, respectively.

From 1983 to 1985, he was a Visiting Scholar at the EECS Department, University of California, Berkeley. In 1985, he was appointed as a Chargé de Recherche at CNRS, Gif-sur-Yvette, France, and in 1992, he joined the Biomedical Engineering Institute and the Electrical Engineering Department, École Polytechnique, Montreal, Canada, where he is now a Full Professor. After some work on nonlinear system identification and modeling, his interests moved toward ill-posed problems in signal and image processing.

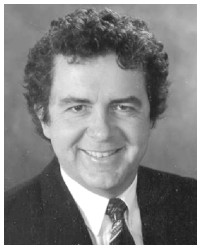

Jean-Jacques Laurin (S'87–M'91–SM'98) received the B.Eng. degree in engineering physics from Ecole Polytechnique de Montreal, Montreal, QC, Canada, and the M.A.Sc. and Ph.D. degrees in electrical engineering from the University of Toronto, Toronto, ON, Canada, in 1983, 1986, and 1991, respectively.

In 1991, he joined the Poly-Grames Research Centre, Ecole Polytechnique de Montreal, where he is currently a Professor. He was an Invited Professor at Ecole Polytechnique Fédérale de Lausanne (EPFL) from 1998 to 1999 and a Visiting Scientist at ESA/ESTEC in 2008. His research interests include antenna design and modeling, near-field antenna measurement techniques, microwave tomography, and electromagnetic compatibility.